Comparison of optical methods for surface roughness characterization

Feidenhans'l, Nikolaj Agentoft; Hansen, Poul Erik; Pilny, Lukas; Madsen, Morten H.; Bissacco, Giuliano; Petersen, Jan C.; Taboryski, Rafael J.

Published in:
Measurement Science and Technology

Link to article, DOI:
10.1088/0957-0233/26/8/085208

Publication date:
2015

Document Version
Publisher's PDF, also known as Version of record

Comparison of optical methods for surface roughness characterization

2015 Meas. Sci. Technol. 26 085208

(http://iopscience.iop.org/0957-0233/26/8/085208)

OPEN ACCESS
IOP Publishing
Measurement Science and Technology
Meas. Sci. Technol. **26** (2015) 085208 (10pp)
doi:10.1088/0957-0233/26/8/085208

Comparison of optical methods for surface roughness characterization

Nikolaj A Feidenhans'l[1,2], Poul-Erik Hansen[1], Lukáš Pilný[3], Morten H Madsen[1], Giuliano Bissacco[3], Jan C Petersen[1] and Rafael Taboryski[2]

[1] Danish Fundamental Metrology A/S, Matematiktorvet 307, Kgs. Lyngby, Denmark
[2] DTU Nanotech, Technical University of Denmark, Kgs. Lyngby, Denmark
[3] DTU MEK, Technical University of Denmark, Kgs. Lyngby, Denmark

E-mail: jcp@dfm.dk and rata@nanotech.dtu.dk

Received 8 April 2015, revised 8 May 2015
Accepted for publication 22 May 2015
Published 16 July 2015

Abstract

We report a study of the correlation between three optical methods for characterizing surface roughness: a laboratory scatterometer measuring the bi-directional reflection distribution function (BRDF instrument), a simple commercial scatterometer (rBRDF instrument), and a confocal optical profiler. For each instrument, the effective range of spatial surface wavelengths is determined, and the common bandwidth used when comparing the evaluated roughness parameters. The compared roughness parameters are: the root-mean-square (RMS) profile deviation (Rq), the RMS profile slope (Rdq), and the variance of the scattering angle distribution (Aq). The twenty-two investigated samples were manufactured with several methods in order to obtain a suitable diversity of roughness patterns.

Our study shows a one-to-one correlation of both the Rq and the Rdq roughness values when obtained with the BRDF and the confocal instruments, if the common bandwidth is applied. Likewise, a correlation is observed when determining the Aq value with the BRDF and the rBRDF instruments.

Furthermore, we show that it is possible to determine the Rq value from the Aq value, by applying a simple transfer function derived from the instrument comparisons. The presented method is validated for surfaces with predominantly 1D roughness, i.e. consisting of parallel grooves of various periods, and a reflectance similar to stainless steel. The Rq values are predicted with an accuracy of 38% at the 95% confidence interval.

Keywords: angle-resolved scattering (ARS), scatterometry, surface roughness, bi-directional reflection distribution function (BRDF), optical profilometry, confocal microscopy

(Some figures may appear in colour only in the online journal)

1. Introduction

Accurate characterization of nanoscale surface roughness is important in many applications, and a number of techniques exist for this purpose [1, 2]. The various characterization techniques, however, are often optimal for different applications or stages of a process [1], hereby requiring that the measured values are comparable between the instruments. However, comparison of values obtained with different instruments is not a simple task, as the design of each instrument imposes different limitations to the measurement bandwidth [1, 3]. This is an often overlooked effect when comparing roughness values [2, 4]. Hence, to perform a reliable comparison of values obtained with different instruments, a study of the accuracy and limits of each method is required.

Two methods often used for roughness measurements are stylus profilers and atomic force microscopy (AFM) [1–3, 5]. Both are mechanical methods, where a sharp tip is traced along the surface and the surface profile assessed from its movement. AFMs generally have only weak interaction forces with the surface, while stylus profilers are known to damage the surface due to excessive forces, resulting in incorrect values and abrasion of the sample, which might not be realized [1, 5]. Compared to mechanical methods, non-contact optical methods are advantageous due to their non-abrasive nature, and the feasibility of some methods to scan large areas in short time. The non-abrasive feature is particularly relevant for very smooth surfaces with roughness in the nanometer range.

In this study, three optical surface characterization methods are analyzed and compared. The comparison is performed in terms of the ISO standardized [6] roughness parameters Rq and Rdq, and the industry standard [7] Aq. The three characterized instruments are: 1) A laboratory scatterometer which measures the angular distribution of light scattered from a surface, quantified by the bi-directional reflection distribution function (BRDF). It evaluates all three roughness parameters. This instrument will be referred to as the 'BRDF instrument'. 2) A commercial scatterometer also measuring the light scattering but in a restricted angular range and with lower resolution. By default it only determines the Aq parameter. It will be referred to as the 'rBRDF instrument' (restricted-BRDF). 3) A commercial optical profiler which uses a confocal technique to acquire a three-dimensional (3D) map of the surface. It evaluates the Rq and Rdq parameters. BRDF and confocal instruments are well-known for roughness characterization [2, 8–10], while the rBRDF instrument is less known, but well described [7, 11–14].

Generally, all characterization methods perform an intrinsic filtering, which define the bandwidth of spatial surface wavelengths from which the measured values are evaluated [1, 4]. For mechanical methods the bandwidth filtering is generally due to the tip radius and scan area [1, 4], while for optical methods it is mainly due to angular constraints in the detection system [2, 4]. This study will determine the filtering bandwidths for each of the three methods, and ensure that values are only compared within common bandwidths. Without establishing the limiting bandwidth for each method, it is inappropriate to compare the measured values, since one method may describe the roughness on a different length scale than the others [4].

Previous studies have mainly compared BRDF instruments with other methods using the power spectral density (PSD) curves rather than the roughness values [15–18], while other studies used smoother samples [2, 5]. One study compared Rq roughness obtained from BRDF and AFM [19], but here only three samples were used and the bandwidth limitations not considered. Another study correlated the RMS roughness with the variance of the scattering distribution [20], but the analyzed samples were all made from the same manufacturing process.

In this study, the three instruments are compared pairwise; as they do not all determine a common parameter. The BRDF and confocal instruments are compared by the Rq and Rdq parameters, while the BRDF and rBRDF instruments are compared by the Aq parameter. We find one-to-one correlations between the three instruments.

Additionally, we present a relation between the Aq and Rq values, which enables the simple rBRDF instrument to predict the ISO standardized roughness parameter Rq, instead of only the less known industry standard Aq. This is advantageous because the rBRDF instrument is better suited than the two other instrument for applications where *in situ* measurements are required, e.g. during a polishing process. The advantages of the rBRDF instrument includes: ease of use, faster and cheaper operation, and a more robust setup.

2. Experimental methods

2.1. Samples

A total of 22 samples were collected for the study. The samples include 4 steel roughness standards with roughness values certified by the Physikalisch-Technische Bundesanstalt (PTB), 16 samples made from one steel grade but polished to different smoothness levels, and 2 samples made with another steel grade and fabrication method. For characterizing the instruments, a silicon wafer (TP436 Si-100, Topsil Semiconductor Materials A/S, Denmark) was used. The specific manufacturing process of the 16 steel samples is described by Pilný *et al* [21].

The samples are all 1D surfaces, consisting of parallel grooves in a wide range of spatial frequencies. Such surfaces have all the roughness features along one dimension, resulting in a simple scattering pattern where all light is diffracted into one plane [4].

The rougher samples have a quite inhomogeneous surface quality, resulting in a significant variation of roughness values on the surface. Even though care was taken to measure in the same position with all three instruments, this inhomogeneity will inevitably increase the uncertainty when comparing the roughness values.

2.2. Roughness parameters

A wide range of roughness parameters can be used to describe a given surface [3]. The most common parameters are calculated from line profiles according to the ISO 4287 standard [6], but due to an increased use of 3D profilers a set of complimentary area roughness parameters have been defined in the ISO 25178-2 standard [22]. In this study, the line parameters are used as these are more appropriate for the 1D surfaces analyzed.

The specific parameters used are: Rq, Rdq and Aq. The 'R' parameters are defined in the ISO 4287 standard [6], while the 'Aq' parameter is defined in the VDA2009 directive [7]. The characteristics associated with each parameter are:

- Rq: the root mean square deviation (RMS) of the profile.
- Rdq: the root mean square of the local slope of profile.
- Aq: the variance of the scattered light distribution from a surface.

The formulas for the Rq and Rdq parameters are:

$$\mathrm{Rq} = \sqrt{\frac{1}{n}\sum_{i=1}^{n} Z_i^2}, \quad \mathrm{Rdq} = \sqrt{\frac{1}{n}\sum_{i=1}^{n}\left(\frac{\mathrm{d}Z_i}{\mathrm{d}x}\right)^2}, \qquad (1)$$

where Z_i is the amplitude of point i, n is the number of sample points, and $\mathrm{d}Z_i/\mathrm{d}x$ is the local slope [6]. ISO 4287 further defines that the parameters must be calculated with suitable low-pass (λs) and high-pass (λc) Gaussian filters, defined in spatial wavelengths. The low-pass filter removes noise from the profile, while the high-pass filter divides the profile into a long-ranged waviness pattern, assumed to be the form of the sample, and the actual roughness profile which is used to calculated Rq and Rdq.

The Aq parameter is defined in an industry directive by the German Association of the Automotive Industry (VDA), an association which includes most of the German car manufacturers and suppliers. This parameter is different from the R parameters, as it does not describe the surface profile but instead how the surface scatters light. It is defined as the variance of the distribution of scattered light [7]:

$$\mathrm{Aq} = k\sum (\varphi' - M)^2 \cdot H(\varphi'), \qquad (2)$$

where $H(\varphi')$ is the normalized light distribution, M the center of mass for the distributions, k a scaling factor to ensure a maximum Aq value of 100, and $\varphi' = \tan(\varphi)$ where φ is the scattering angle. However, as presented in a later section, a slight modification of equation (2) is applied, where φ is used instead of φ'.

A low Aq value is a measure of low surface roughness, since smooth samples reflect a narrow beam, while rough samples scatter the light into larger angles.

2.3. BRDF instrument

A scatterometer is used to measure the scattering spectrum from the samples, and from this calculate the bi-directional reflection distribution function (BRDF). The BRDF is a common way of describing the pattern of light scattered from a surface[4] [4]. It is similar to the angle-resolved scatter (ARS), only difference being the cosine factor [4]. The BRDF is given as the ratio between the scattered surface radiance and the incident surface irradiance, corresponding to:

$$\mathrm{BRDF} = \frac{P_\mathrm{s}/\Omega_\mathrm{s}}{P_\mathrm{i}\cos(\theta_\mathrm{s})}, \qquad (3)$$

where P_s is the scattering power in the scattering angle (θ_s), Ω_s the detector solid angle, P_i the incident beam power, and $\cos(\theta_\mathrm{s})$ a correction factor.

The BRDF instrument is illustrated in figure 1. It consists of a 662 nm diode laser (LBX-660-100-CIR-PP, Oxxius, France), which is linearly polarized, shaped with an iris, and focused onto the detector plane with a 500 mm focal length lens (LA4184, Thorlabs Inc. USA). The incident polarization is *s* oriented, with the depolarization in the lens assumed negligible. The scattering intensity (P_s) is detected with a photodetector (New Focus Model 2032, Newport, USA) and a

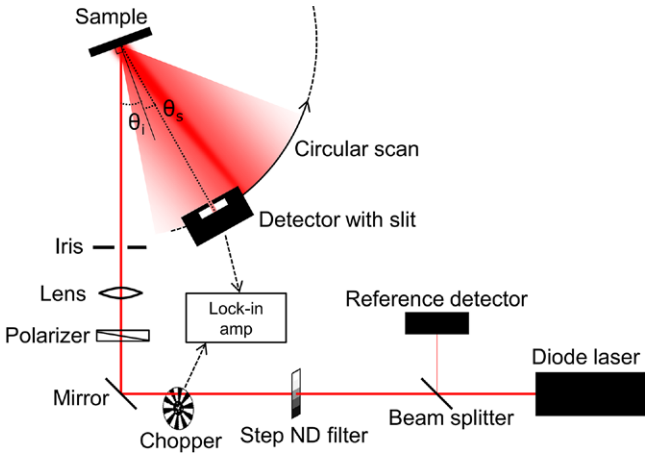

Figure 1. Diagram of BRDF instrument, see description in text.

lock-in amplifier (SR530, Stanford Research Systems, USA) locked to a chopper (SR540, Stanford Research Systems, USA). A rotary stage (NR360S/M, Thorlabs Inc. USA) scans the detector along the in-plane scattering direction, with steps between 0.01° and 0.16°. The detector is positioned 350 mm from the sample surface and shielded with a slit of 215.5 μm × 3.04 mm, resulting in a detector solid angle of Ω_s = 5.343 μsr. The laser intensity is monitored using a beam splitter and a photodetector (New Focus Model 2032, Newport, USA), while a step neutral density (ND) filter (NDL-10 S-4, Thorlabs Inc. USA) decreases the beam intensity if needed. The resulting dynamic range is approximately 8 orders of magnitude, with a noise floor around $10^{-4}\mathrm{sr}^{-1}$. The measured intensities are scaled relative to the laser intensity and corrected for the ND filters used. The incident intensity (P_i) is determined by a straight through scan without a sample. One scan, with an angle of incidence (AOI) of 10°, was acquired for each sample and the data analyzed in Matlab (Matlab R2014b, MathWorks, USA).

The dominant sources of uncertainty in the BRDF measurement are the ND filter transmissions, the angular accuracy of the detector, and the linearity of the detector and amplifier system.

The standard uncertainty (SU) on the intensity, P_s, were estimated to 5.7%, 3.9%, 1.0%, for the three factors respectively. From error propagation [23], this results in a combined SU of 6.1%. This uncertainty was applied to all P_s and P_i values, and the resulting variation in Rq and Aq value assigned as the SU on these values.

2.3.1. Bandwidth limits. The BRDF instrument is bandlimited by six factors: the angular range of the scan, the laser wavelength, the beam size on the sample, the slit width, the angular resolution, and the beam width in the detector plane. The limits are mainly imposed by the diffraction angle of surface features with specific spatial wavelengths, governed by the diffraction equation[5] [4]:

$$\sin\theta_\mathrm{s} - \sin\theta_\mathrm{i} = \lambda f, \qquad (4)$$

[4] Section 1.5 in [4].
[5] Section 1.2 in [4].

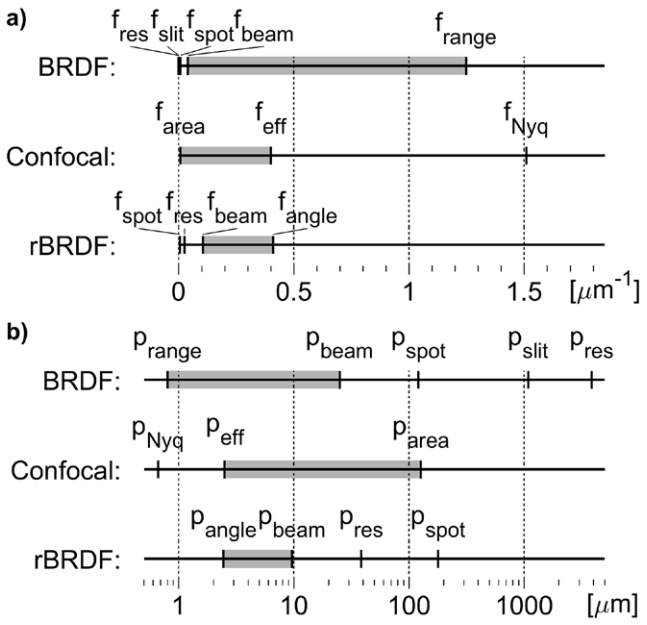

Figure 2. Comparison of the frequency limits of the three instruments, (a) in spatial frequency unit, and (b) in spatial wavelengths. The gray rectangles show the resulting bandwidth for each instrument. Note the log scale in (b).

where θ_s is the scattering angle, θ_i the incident angle, λ the incident wavelength, and f the spatial frequency of the scattering structures.

In the following, each limiting factor is presented and the final bandwidth of the BRDF instrument determined. A comparison of the limits for all three instruments is seen in figure 2.

1: The angular scan range is a high frequency limit (low-pass filter), since high frequent structures scatter into large angles. The scan range limit is when the detector reaches the sample plane, which for an AOI of 10° is 80° from the specular angle. The corresponding frequency is found from equation (4) to $f_{\text{max, range}} = (\sin(10° + 80°) - \sin(10°))/662\,\text{nm} = 1.25\,\mu\text{m}^{-1}$. This limit could be increased by using a larger AOI and then measure the backwards reflected side of the spectrum, but a small AOI is preferred to ease comparison with the rBRDF instrument.

2: The laser wavelength is also a high frequency limit. It is based on the property of the diffraction equation, that spatial frequencies longer than $1/\lambda_{\text{laser}}$ cannot scatter [24] because the angles would be above 90°. This results in $f_{\text{max, wave}} = 1/662\,\text{nm} = 1.51\,\mu\text{m}^{-1}$.

3: The beam size on the sample is a low frequency limit (high-pass filter), since spatial wavelengths longer than the spot diameter do not diffract. Actually, several periods within the spot are needed to provide a sufficiently intense diffraction pattern [25]. The beam width is determined to 600 μm at the $1/e^2$ intensity point, using a beam profiler (SP620U, Ophir Optronics, USA) placed at the sample position. Requiring five periods within this length results in $f_{\text{min, sample}} = 1/(600\,\mu\text{m}/5) = 0.0083\,\mu\text{m}^{-1}$.

4 + 5: The slit width and angular resolution both constitute low frequency limits, because scattering features below these limits are indistinguishable in the spectrum. In angular terms the limits are 0.035° and 0.01°, which from equation (4) corresponds to the frequencies $f_{\text{min, slit}} = (\sin(10° + 0.035°) - \sin(10°))/662\,\text{nm} = 0.00092\,\mu\text{m}^{-1}$ and $f_{\text{min, resolution}} = (\sin(10° + 0.01°) - \sin(10°))/662\,\text{nm} = 0.00026\,\mu\text{m}^{-1}$, respectively.

6: The beam width in the detector plane is also a low frequency limit, as scattering from long spatial wavelengths are buried in the intense specular peak. Based on a straight-through scan of the beam, the $1/e^2$ width was found to: $\theta_{\text{beam}} = 0.111°$, which by equation (4) corresponds to $f_{\text{min, beam}} = (\sin(10° + 0.111°) - \sin(10°))/662\,\text{nm} = 0.0029\,\mu\text{m}^{-1}$. However, during the further analysis this beam width was found too small, as the incident beam still held a significant intensity outside this range, which influenced the roughness calculations. Instead, the effective beam width was determined by comparing the straight-through beam with its reflection from a mirror (10Z20AL.2, Newport Corporation, USA), and estimating the angle where the two curves started to deviate. This width was found to $f_{\text{min, beam effective}} = 0.04\,\mu\text{m}^{-1}$, corresponding to $\theta = 1.54°$. This limit was applied to all BRDF spectra, but it should be seen as a worst-case scenario mainly relevant for very smooth samples.

The resulting frequency bandwidth of the BRDF instrument is $0.04\,\mu\text{m}^{-1}$–$1.25\,\mu\text{m}^{-1}$.

2.3.2. Calculation of roughness parameters. The root-mean-square roughness (Rq) and root-mean-square slope (Rdq) are calculated from the BRDF spectrum using the Rayleigh–Rice (RR) theory [4, 26]. Other possibilities include the Generalized Harvey–Shack (GHS) theory [27] and the Beckmann–Kirchhoff theory [28], but the RR theory is used because it is the most well-known and widely accepted scattering theory [4, 27, 29]. The analyzed samples have Rq values in the range 2 nm–49 nm, which exceeds the traditional limit for the RR theory of the surface being 'optically smooth', defined as[5] [4]:

$$\left(\frac{4\pi\cos(\theta_i)\sigma}{\lambda}\right)^2 \ll 1, \tag{5}$$

where σ is the total RMS roughness with no bandwidth limits, θ_i the angle of incidence, and λ the wavelength of the incident light. However, equation (5) is simply a Taylor expansion of the original equation [30, 31], and it is this approximation which introduces the assumption of $\text{Rq}/\lambda \ll 1$. Hence the surface roughness is not limited by equation (5), as also found by other studies [30, 32].

Because all samples are 1D surfaces with purely in-plane scattering, the PSD curves are evaluated from the BRDF as 1D PSD curves, as described by Stover[6] [4]. From these, the Rq and Rdq values are determined by integration, with integration limits defined by the frequency bandwidth. For the refractive index of the steel samples, a tabular value of

[6] Section 4.3 in [4].

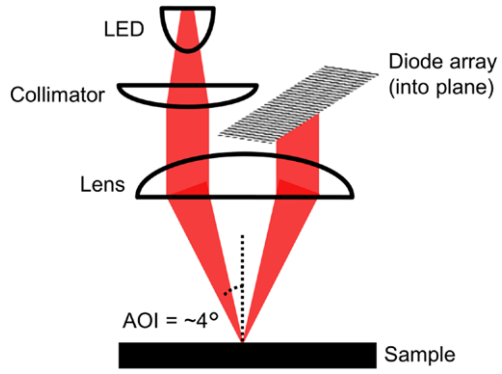

Figure 3. Approximate diagram of the rBRDF instrument, based on published device illustrations [7, 11–14] and own analysis.

$\tilde{n}_{\text{steel}} = 2.55 + 4.32i$ is used [33]. The value might be slightly different for our samples, but small changes in the refractive index were found to be negligible for calculating the Rq value. For the silicon sample a value of $\tilde{n}_{\text{Si}} = 3.82 + 0.015i$ is used [34].

The Aq value is determined from the scattering spectrum, as defined in the VDA directive [7]. However, for an AOI of 10° the BRDF instrument is limited to measure the one-sided scattering spectrum, hence the scattering spectrum is mirrored along the specular direction, to provide the full two-sided peak needed for the Aq calculation. When calculating the restricted angle Aq value, the scattering spectrum is cropped to the desired angular range.

2.4. rBRDF instrument

The commercial scatterometer is an OptoSurf OS 500–32 (OptoSurf GmbH, Germany), referred to as the 'rBRDF instrument' due to the restricted acceptance angle. It measures the same scattering spectra as the BRDF instrument, but it has a simpler design optimized to provide quality control in industrial manufacturing [35].

The rBRDF instrument has previously been described by others [7, 11–14], and is comprised of a photodiode generating ~670 nm light, a lens which focuses the light into a ~0.9 mm spot on the sample and also collects the reflected light, and lastly a linear photodiode array for detecting the scattering spectrum, see illustration in figure 3. It has an AOI of ~4° perpendicular to the diode array, while the sample tilt is adjusted to ensure an AOI of 0° along the measuring direction. The major differences to the BRDF instrument are: a restricted acceptance angle of only ±16° (corresponding to NA = 0.28), a spectral resolution of 1° due to the angular size of the photodiodes, a dynamic range of around 3 orders of magnitude, the focus point on the sample instead of the detector.

These differences result in a lower resolution of the scattering spectra, and no information on the wide angle scattering from features with wavelengths below a few micrometers. The advantages on the other hand, are a more compact instrument and much faster measurements, in the range of milliseconds. Due to the high measurement speed, it is possible to measure the Aq value of many locations on a surface to generate a 2D map of the surface roughness [21].

The standard measurement output is: the Aq value, the total light intensity detected, and the scattering distributions center of mass. In this study, however, the raw intensity data from the diode array was extracted, and the Aq value calculated using a custom Matlab script. For each sample, between five and ten measurements were performed close to the beam position in the BRDF measurement, the number depending on the homogeneity of the surface quality. From these measurements the average Aq value was determined, and the uncertainty estimated as the standard error of the mean (SEM).

During the analysis, a small correction was made to the Aq formula in equation (2). Based on the raw rBRDF spectra, Aq values were calculated in Matlab as described in the VDA directive and compared to the Aq value provided by the OptoSurf control software. This revealed a consistently smaller Aq value than provided by the OptoSurf software, though the deviations did not exceeded 5%. The deviation was reduced to below 0.4%, by replacing the VDA defined x value of $\tan(\varphi)$ with the angle φ directly. When calculating Aq values in the further analysis, the slightly modified formula using φ as x values is used.

2.4.1. Bandwidth limits.

The limiting factors in the rBRDF instrument are a high frequency limit imposed by the acceptance angle, and three low frequency limits imposed by the resolution of the diode array, the beam width on the detector, and the beam spot size on the sample.

The high frequency limit is determine by the ±16° acceptance angle, which by equation (4) corresponds to $f_{\text{max, angle}} = (\sin(16°) - \sin(0°))/670\,\text{nm} = 0.411\,\mu\text{m}^{-1}$. The low frequency limits are similarly found to: $f_{\text{min, res}} = (\sin(1°) - \sin(0°))/670\,\text{nm} = 0.0260\,\mu\text{m}^{-1}$, $f_{\text{min, beam}} = (\sin(4°) - \sin(0°))/670\,\text{nm} = 0.104\,\mu\text{m}^{-1}$, $f_{\text{min, sample}} = 1/(900\,\mu\text{m}/5) = 0.0056\,\mu\text{m}^{-1}$, for the resolution, the beam width on the detector and on the sample, respectively.

Since calculation of the Aq value requires the specular component, the spectra are not cropped with the low frequency limits.

2.5. Optical profiler

The optical profiler is a 3D confocal interference microscope (Sensofar PLu Neox, Sensofar Tech, Spain) equipped with a 50 × (NA 0.80) objective. It is capable of both confocal and white light interferometry, but only the confocal technique with 460 nm light is used in this study. The measurement output is a high resolution 3D profile of the surface, with a field of view of 254.6 μm × 190.9 μm and an image size of 768 pixels × 576 pixels [36]. All samples are aligned with the line structures perpendicular to the long image axis.

2.5.1. Bandwidth limits.

The confocal microscope is, like all profiling tools, restricted by the pixel resolution and the size of the scanned area [37]. The pixel resolution provides a high frequency limit, while the scan area limits the low frequencies. The scan area limit is determined by requiring two periods within the image $f_{\text{min, area}} = 1/(L_{\text{scan range}}/2) = 1/(254.6\,\mu\text{m}/2) = 0.0079\,\mu\text{m}^{-1}$. By applying the Nyquist

sampling theorem of two samples per period, the pixel resolution limit is found to $f_{\text{max, Nyq}} = n_{\text{pixels}}/(2L_{\text{scan range}}) = 768/(2 \times 254.6\,\mu\text{m}) = 1.51\,\mu\text{m}^{-1}$. The microscope is also limited by the acceptance angle of the objective, as high frequency features scatter outside the objective. The numerical aperture (NA) describe the largest collection and incident angles of the objective, corresponding to a frequency limit found from equation (4) $f_{\text{max, NA}} = (\text{NA} + \text{NA})/\lambda = (2 \times 0.8)/460\,\text{nm} = 3.48\,\mu\text{m}^{-1}$. In addition, the microscope might include apertures or other restrictions to the light path, which would lower the actual frequency limit.

However, the Nyquist frequency is the limiting frequency at which the spatial period information is just preserved, whereas the limit at which also the waveform is sufficiently preserved is somewhat higher. Hence the effective spatial frequency limit is lower than the Nyquist frequency, and was determined experimentally. PSD curves calculated from the confocal 3D profiles were compared with the BRDF scan and an AFM image (Park NX20, Park Systems, South Korea). At a frequency of approximately $0.4\,\mu\text{m}^{-1}$ and onwards, the confocal microscope was found to deviate significantly from the other PSDs, hence this is the effective frequency limit after which the waveform is not sufficiently preserved. An effective frequency limit of $f_{\text{max, eff}} = 0.4\,\mu\text{m}^{-1}$ equals a spatial wavelength of $2.5\,\mu\text{m}$ with 7.6 pixels per period, which corresponds well with previous studies that found that around six to ten sample points (pixels) per period are needed to accurately determine the roughness values [5, 38].

The resulting bandwidth of the confocal microscope is $0.0079\,\mu\text{m}^{-1}$–$0.4\,\mu\text{m}^{-1}$.

2.5.2. Calculation of roughness parameters. Based on the 3D surface profiles the Rq and Rdq values are calculated as defined in ISO 4287, using the image processing software SPIP (SPIP ver. 6.3.2, Image Metrology, Denmark). The bandwidth limit is applied using the λs and λc filters, where $\lambda = 1/\text{f}$.

Confocal images were acquired from five positions on each sample. The positions were chosen close to the beam position during the BRDF measurement to decrease the effect of the inhomogeneous surface quality. The measurement uncertainty was estimated as the standard error of the mean (SEM).

3. Results and discussion

3.1. BRDF and confocal comparison

The BRDF and confocal instruments are compared in terms of the Rq and Rdq parameters, evaluated in the bandwidth (f_{min}–f_{max}): $0.04\,\mu\text{m}^{-1}$–$0.4\,\mu\text{m}^{-1}$, corresponding to λs = $2.5\,\mu$m and λc = $25\,\mu$m. As seen in figure 4, both the Rq and Rdq values show a one-to-one correlation between the two instruments. The large uncertainties on the confocal values are due to the inhomogeneous surface quality of the samples, resulting in noticeable deviations between the five measurement positions. The uncertainties on the BRDF values are more constant, as these are only measured in one position,

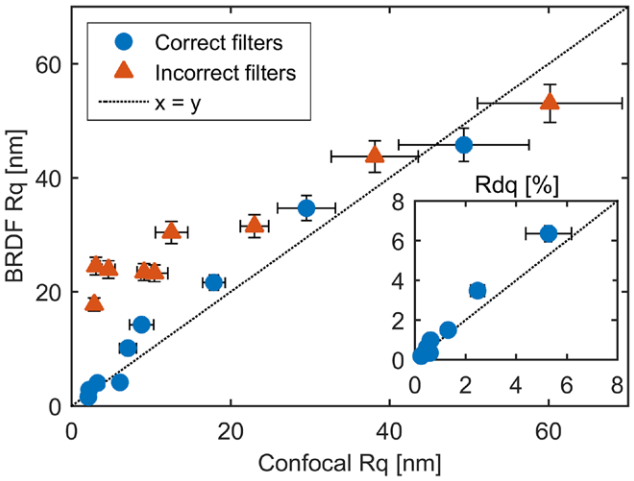

Figure 4. Comparison of Rq obtained from the BRDF and confocal instruments, with the corresponding Rdq comparison shown in the insert. One-to-one correlations between the instruments are seen, but only with correct filtering. For this comparison, a subset of only 9 samples was used. Error bars represent ±1 SEM on the *x* values, and ±1 standard uncertainty (SU) on the *y* values.

and instead based on an estimation of the uncertainty of the intensity measurements.

To stress the importance of applying the correct filters, Rq values obtained using some improper filters are also shown in figure 4, and the correlation is seen to be significantly reduced. These filters are determined as the FWHM diameter of the beam and the full scan range, $0.0015\,\mu\text{m}^{-1}$–$1.25\,\mu\text{m}^{-1}$, while the confocal images are filtered to the minimum and maximum values allowed by ISO 4287, λs = $0.8\,\mu$m and λc = $80\,\mu$m.

The good correlation reveal that the RR theory continues to provides correct roughness values for all samples in the study, hence this study supports the conclusions of Harvey *et al* [30] and Stover *et al* [32], that the smoothness requirement is not limited by equation (5).

3.2. BRDF and rBRDF comparison

The BRDF and rBRDF instruments are compared by the Aq parameter with the common frequency range defined by the restricted opening angle of ±16°, corresponding to $f_{\text{max}} = 0.4\,\mu\text{m}^{-1}$ and no minimum frequency. It is found that the frequency filter alone is not enough to ensure comparable values between the two instruments. Before calculating the Aq value, a smoothing function is required for the BRDF spectrum, to simulate the effects on the scattering spectra imposed by the different designs of the two instruments. The crucial differences in this context are the focus point and beam divergence of the incident light. In the BRDF instrument, the incident light is a laser beam focused into a small spot on the detector, where a slit limits the detector width to only 0.035° ($215.5\,\mu$m), hereby resulting in a very high resolution of the scattering spectrum. The rBRDF instrument on the other hand, uses an LED source which is focused onto the sample, thereby resulting in a significant beam divergence on the detector. Furthermore, the size of each diode in the detector array is

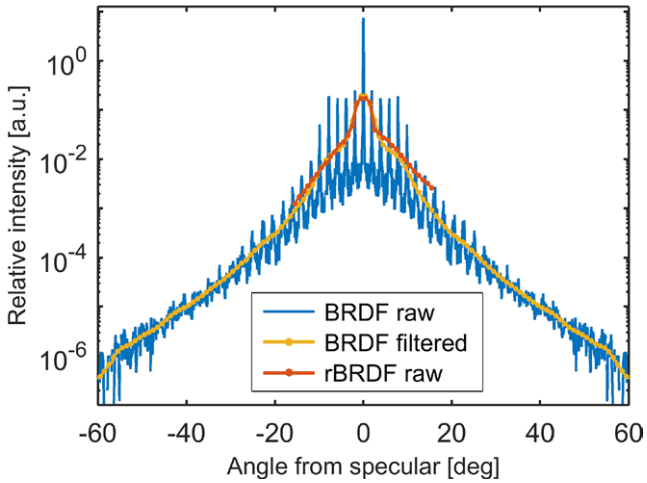

Figure 5. Scattering spectra obtained by BRDF and rBRDF instruments. The distinct spikes on the raw BRDF spectrum are caused by a periodic surface feature of 20 μm, resulting from the polishing process. The spectra are scaled relative to the area under each curve, and the BRDF spectra shown before cropping.

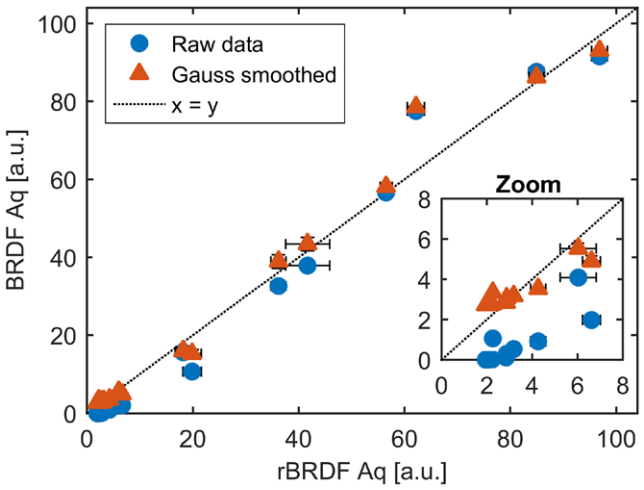

Figure 6. Comparison of Aq values obtained from the BRDF and rBRDF instruments. A strong correlation between the values is seen, but only after applying the Gaussian smoothing and the frequency filter of $f_{max} = 0.4\,\mu m^{-1}$. Error bars represent ±1 SEM on the x values, and ±1 SU on the y values.

around 1°. Consequently, for comparing the two instruments, the high resolution BRDF spectrum is smoothened and binned into 1° intervals.

The smoothing function is a sum of three Gaussians, as suggested by Karamehmedović *et al* [39], determined by a fit to the distribution of light reflected from a silicon wafer, which provides the narrowest peak measureable by the rBRDF instrument. The function has the form:

$$f(x) = \sum_{i=1}^{3} A_i \exp\left(-\frac{(x-\mu_i)^2}{(2\sigma_i)^2}\right), \qquad (6)$$

with the parameters: A_{1-3} = (0.295; 0.0562; 0.000621), μ_{1-3} = (0.198; 0.0200; 0.102), σ_{1-3} = (1.41; 1.53; 5.55). The filter is applied by convoluting the function with the raw scatter data, binning the spectrum into 1° intervals, and cropping it to a range of ±16° from specular.

As seen in figure 5, the raw spectra from the BRDF and rBRDF instruments are quite different, but by applying the Gaussian function to the BRDF data the two spectra become comparable. The change in Aq value for the spectrum shown in figure 5 is from 10.7 to 15.3, between the raw and filtered spectrum, respectively.

A comparison of the Aq values obtained from the BRDF and rBRDF instruments is seen in figure 6. The filtered values (triangular dots) show a good correlation between the two instruments, with only a single outlier at (62, 78), probably resulting from the inhomogeneous surface quality. If the Gaussian filter is not applied (round dots), the Aq values are consistently underestimated.

3.3. Aq and Rq relation

With the strong correlation between the three instruments, we now turn to explore the capabilities of the simplest device: the rBRDF instrument.

The main limitations of this device are that it only evaluates the Aq parameter, and only for an angular range of ±16°, which essentially removes all information of spatial wavelengths below 2.5 μm. In the following, we present a method to predict the Rq value for a wider frequency range, using the rBRDF Aq value and a calibration of the incident light intensity. The first step is to extrapolate the full range Aq value from the restricted one, followed by a conversion to the full range Rq value. In this context, the 'full range' refers to the full frequency bandwidth of the BRDF instrument of $0.04\,\mu m^{-1}$–$1.25\,\mu m^{-1}$, while the 'restricted range' is the ±16° acceptance angle of the rBRDF instrument.

Figure 7(a) shows a comparison of the three Aq values: the rBRDF Aq values (Aq_{rBRDF}), the BRDF restricted Aq values (Aq_{16deg}), and the BRDF full range Aq values (Aq_{80deg}). It is seen that while the Aq_{16deg} values corresponds linearly to the Aq_{rBRDF} values, as also shown in figure 6, the Aq_{80deg} values diverge significantly from this trend. The rapid increase in Aq_{80deg} is caused by the rough samples scattering increasing amounts of light outside the ±16° range, while the smooth samples with low Aq_{rBRDF} values scatter all light into the restricted angular range. The Aq_{80deg} values can exceed the normal limit of 100, because the k factor is kept constant while evaluating the wide angular range.

By calibrating the incident intensity of the rBRDF instrument, the intensity loss for each sample is determined from the detected intensity, and the loss compared to the difference in Aq value (Aq_{80deg}–Aq_{16deg}), see figure 7(b). These two values are expected to correlate, as they both describe the scattering intensity outside the ±16° interval. The incident intensity is calibrated from the reflected intensity of a silicon wafer, which is converted to incident intensity from the refractive index [34] and the Fresnel reflectance.

Figure 7(b) reveals a strong correlation between the two values, fitted with a second order polynomial using least squares. This correlation enables an extrapolation from Aq_{rBRDF} to Aq_{80deg}, but it should only be applied to rough

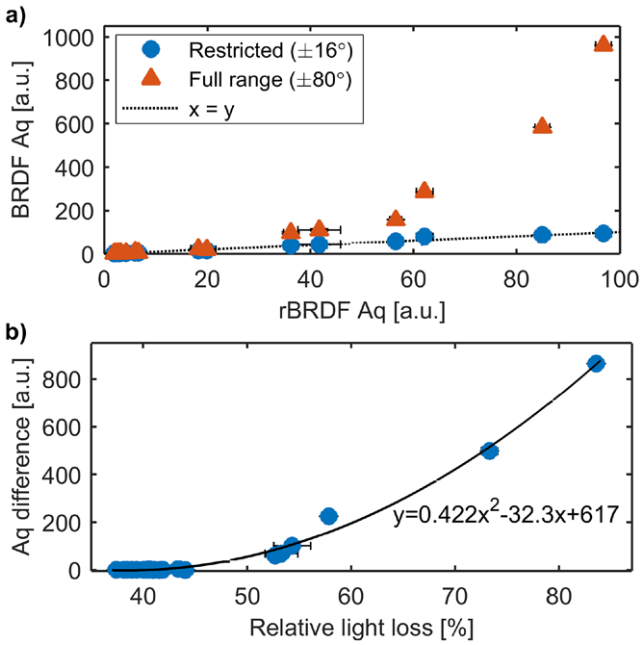

Figure 7. (a) Relation between the Aq_{rBRDF}, Aq_{16deg}, and Aq_{80deg} values. (b) Comparison of the difference in Aq value (Aq_{80deg}–Aq_{16deg}) with the relative intensity of light lost outside the restricted range. The lowest loss is not zero because the reflectance of the steel is only ~67%. Error bars represent ±1 SEM on the *x* values, and ±1 SU on the *y* values.

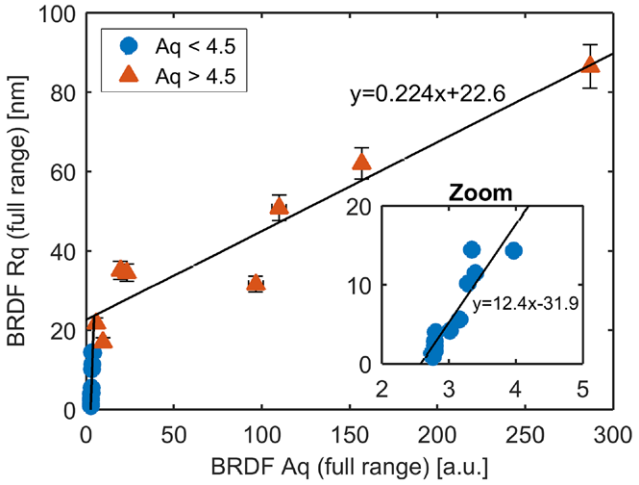

Figure 8. Comparison of Rq and Aq_{80deg} values obtained from the BRDF measurements, showing two regimes of linear correlation, fitted using least squares. Error bars represent ±1 SU on both *x* and *y* values.

samples with significant scatter outside the ±16° range, defined as $Aq_{rBRDF} > 10$. Since the relation in figure 7(b) is based on the relative light loss of stainless steel samples, the presented polynomial coefficients are only valid for materials with a reflectance similar to $R_{steel} = 33\%$. However, by accounting for the material absorbance and using the 'relative *scattering* loss' instead of the total (scattering + absorbance) loss, this procedure will also be valid for other materials.

Following the Aq extrapolation, figure 8 shows a comparison of the full range Aq_{80deg} values with the Rq values from the full bandwidth of the BRDF instrument, $0.04\,\mu m^{-1}$–$1.25\,\mu m^{-1}$. Figure 8 reveals a good correlation between the Aq_{80deg} and Rq values, with two regimes of linear correlations: for rough samples with $Aq_{80deg} > 4.5$, and for smooth samples with $Aq_{80deg} < 4.5$ (the corresponding Rq limit is around 17 nm). The regimes are both fitted with first order polynomials using least squares. The presence of the two linear regimes could indicate a transition from mainly specular to more diffuse reflection, since the raw BRDF spectra of the smooth samples were significantly sharper and had a more pronounced specular peak, compared to the samples in the rough regime.

By combining the linear relations with the parabolic Aq extrapolation presented in figure 7, the ISO standardized Rq roughness of a surface can be predicted from the Aq_{rBRDF} value and the total light intensity, both quantities provided by the rBRDF software. To our knowledge, such a relation has not been reported before, as previously the Aq parameter was only known to correlate with roughness parameters after a calibration to each specific process [7, 12]. Since several samples with different roughness are analyzed in this study, we expect that the presented relations at least are valid for most 1D steel surfaces made by a directional processes, such as milling, grinding, or unidirectional polishing. This assumption is supported by the fact that many surfaces show similar scattering behavior [40–44], described by general functions like the K-Correlation (also called the ABC model) [24, 27] or the widely used ABg model [43]. For all samples in this study, the ABg model provides good fits to the spectra, hereby indicating that the results are applicable for other surfaces with similar scattering spectra. Extending the analysis to 2D surfaces where the roughness features are no longer parallel but are randomly distributed is straight forward. The scattering pattern then changes from a purely in-plane scattering to a 2D spectrum, in principle requiring a full hemispherical BRDF scan, and the Rq value must then be calculated along a certain direction or be replaced by the equivalent area parameter Sq defined in ISO 25178-2.

To test the accuracy of the Rq prediction, it is applied to the rBRDF data from the 22 samples, and the estimated Rq values compared to the full range BRDF Rq values ($0.04\,\mu m^{-1}$–$1.25\,\mu m^{-1}$). The average absolute deviation is 7%, with a standard deviation of 15 percentage points. Hence, the presented relations can determine the Rq value with an accuracy of 38%, at the 95% confidence interval.

4. Conclusion

Three instruments for characterization of nanoscale surface roughness have been examined for correspondence between the parameters Rq, Rdq and Aq. For each instrument, the range of spatial surface wavelengths in-which the roughness values were correctly evaluated, was determined. The analysis is performed in spatial frequency space, hence the ranges are given as a frequency bandwidth for each instrument (f_{min}–f_{max}): BRDF instrument: $0.04\,\mu m^{-1}$–$1.25\,\mu m^{-1}$, rBRDF instrument: $0.104\,\mu m^{-1}$–$0.41\,\mu m^{-1}$, confocal microscope: $0.0196\,\mu m^{-1}$–$0.4\,\mu m^{-1}$, see overview in figure 2. These

bandwidths were applied to only compare roughness values within common frequency ranges.

The BRDF instrument and confocal microscope were compared in terms of the Rq and Rdq parameters, and showed a one-to-one correspondence in both parameters for the frequency range $0.04\,\mu m^{-1}$–$0.4\,\mu m^{-1}$, see figure 4.

The BRDF and rBRDF instruments were compared in terms of the Aq parameter. By including a Gaussian smoothing function to compensate for the instrument differences, the Aq values showed a one-to-one correspondence, see figure 6.

A relation between the rBRDF Aq values and the BRDF Rq values was determined, hereby enabling the rBRDF instrument to also measure the Rq parameter. The conversion is based on a second order polynomial, $y = ax^2 + bx + c$, to obtain the wide range Aq_{80deg} from the restricted range Aq_{rBRDF}, followed by a conversion of Aq_{80deg} to the Rq value through a first order polynomial relation, $y = dx + e$. The polynomial coefficients were found to be: $a = 0.422$, $b = -32.3$, $c = 617$, $d_{smooth} = 12.4$, $e_{smooth} = -31.9$, $d_{rough} = 0.224$, $e_{rough} = 22.6$, where the 'smooth' and 'rough' subscripts refer to two regimes of linear correlation, see figure 8. Note that the polynomials are only applicable for certain levels of surface roughness. The crossover between the 'smooth' and 'rough' linear regimes is at $Aq_{80deg} = 4.5$, while the second order polynomial should be applied to samples with $Aq_{rBRDF} > 10$. The conversion from Aq_{rBRDF} to Rq is achieved with an accuracy of 38%, at the 95% confidence interval.

Acknowledgments

The authors acknowledge financial support from the Danish Ministry of Higher Education and Science through the Industrial PhD Programme, and the EC FP7 collaborative project 'IFaCOM' (Project no. NMP-FoF 285489).

References

[1] Whitehouse D J 1994 *Handbook of Surface Metrology* (Bristol: IOP Publishing Ltd)
[2] Duparré A, Ferre-Borrull J, Gliech S, Notni G, Steinert J and Bennett J M 2002 Surface characterization techniques for determining the root-mean-square roughness and power spectral densities of optical components *Appl. Opt.* **41** 154–71
[3] De Chiffre L, Lonardo P, Trumpold H, Lucca D A, Goch G, Brown C A, Raja J and Hansen H N 2000 Quantitative characterisation of surface texture *CIRP Ann. Manuf. Technol.* **49** 635–52
[4] Stover J C 2012 *Optical Scattering: Measurement and Analysis* (Bellingham, WA: SPIE Press)
[5] Poon C Y and Bhushan B 1995 Comparison of surface roughness measurements by stylus profiler, AFM and non-contact optical profiler *Wear* **190** 76–88
[6] International Organization for Standardization 1998 *ISO 4287: Geometrical Product Specifications (GPS)—Surface Texture: Profile Method: Terms, Definitinos and Surface Texture Parameters* (Geneva: International Organization for Standardization (ISO))
[7] Verband der Automobilindustrie E.V. (VDA) 2010 *VDA 2009:2010-07—Angle-Resolved Light Scattering Measurement* (Berlin: Verband der Automobileindustrie (VDA))
[8] Udupa G, Singaperumal M, Sirohi R S and Kothiyal M P 2000 Characterization of surface topography by confocal microscopy: I. Principles and the measurement system *Meas. Sci. Technol.* **11** 305–14
[9] Mauch F and Osten W 2014 Model-based approach for planning and evaluation of confocal measurements of rough surfaces *Meas. Sci. Technol.* **25** 105002
[10] Jordan H-J, Wegner M and Tiziani H 1999 Highly accurate non-contact characterization of engineering surfaces using confocal microscopy *Meas. Sci. Technol.* **9** 1142–51
[11] Brodmann R and Allgauer M 1989 Comparison of light scattering from rough surfaces with optical and mechanical profilometry *Proc. SPIE 1009, Surface Measurement and Characterization, 111* ed J M Bennett pp 111–8
[12] Brodmann R and Seewig J 2013 *Encyclopedia of Tribology: Springer Reference* ed Q Wang and Y Chung (Berlin, Heidelberg: Springer) doi:10.1007/978-0-387-92897-5_326
[13] Brodmann R and Thurn G 1986 Roughness measurement of ground, turned and shot-peened surfaces by the light scattering method *Wear* **109** 1–13
[14] Brodmann R, Gerstorfer O and Thurn G 1985 Optical roughness measuring instrument for fine-machined surfaces *Opt. Eng.* **24** 243408
[15] Schröder S, Gliech S and Duparré A 2005 Sensitive and flexible light scatter techniques from the VUV to IR regions *Proc. SPIE 5965, Optical Fabrication, Testing, and Metrology II* vol 5965 p 59651B
[16] Ruppe C and Duparré A 1996 Roughness analysis of optical films and substrates by atomic force microscopy *Thin Solid Films* **288** 8–13
[17] Deumié C, Richier R, Dumas P and Amra C 1996 Multiscale roughness in optical multilayers: atomic force microscopy and light scattering *Appl. Opt.* **35** 5583–94
[18] Von Finck A, Herffurth T, Schröder S, Duparré A and Sinzinger S 2014 Characterization of optical coatings using a multisource table-top scatterometer *Appl. Opt.* **53** A259–69
[19] Hüser D, Rinder T and Rothe H 1998 Comparison of PSD measurements using stray light sensors with PSD curves evaluated from topography of large AFM scans *Proc. SPIE—Int. Soc. Opt. Eng.* **3426** 262–72
[20] Lu R-S and Tian G Y 2006 On-line measurement of surface roughness by laser light scattering *Meas. Sci. Technol.* **17** 1496–502
[21] Pilný L, Bissacco G and De Chiffre L 2014 Validation of in-line surface characterization by light scattering in robot assisted polishing *3rd Int. Conf. on Virtual Machining Process Technology (VMPT)*
[22] International Organization for Standardization 2012 *ISO 25178-2:2012: Geometrical Product Specifications (GPS)—Surface Texture: Areal—Part 2: Terms, Definitions and Surface Texture Parameters* (Geneva: International Organization for Standardization (ISO))
[23] Joint Committee for Guides in Metrology 2008 *Evaluation of Measurement Data—Guide to the Expression of Uncertainty in Measurement (JCGM 100:2008)* (Sèvres: Bureau International des Poids et Mesures (BIPM))
[24] Dittman M G 2006 K-correlation power spectral density & surface scatter model *Proc. SPIE 6291, Optical Systems Degradation, Contamination, and Stray Light: Effects, Measurements, and Control II* ed O M Uy *et al* p 62910R
[25] Hirayama K, Glytsis E N and Gaylord T K 1997 Rigorous electromagnetic analysis of diffraction by finite-number-of-periods gratings *J. Opt. Soc. Am.* A **14** 907
[26] Rice S O 1951 Reflection of electromagnetic waves from slightly rough surfaces *Commun. Pure Appl. Math.* **4** 351–78
[27] Krywonos A, Harvey J E and Choi N 2011 Linear systems formulation of scattering theory for rough surfaces with

arbitrary incident and scattering angles *J. Opt. Soc. Am.* **28** 1121–38
[28] Beckmann P and Spizzichino A 1963 *The Scattering of Electromagnetic Waves from Rough Surfaces* (Oxford: Pergamon)
[29] Harvey J E, Krywonos A and Stover J C 2007 Unified scatter model for rough surfaces at large incident and scatter angles *Proc. SPIE 6672, Advanced Characterization Techniques for Optics, Semiconductors, and Nanotechnologies III* vol 6672, ed A Duparré *et al* p 66720C
[30] Harvey J E, Schröder S, Choi N and Duparré A 2012 Total integrated scatter from surfaces with arbitrary roughness, correlation widths, and incident angles *Opt. Eng.* **51** 013402
[31] Bennet J M and Mattsson L 1999 *Introduction to Surface Roughness and Scattering* (Washington, DC: Optical Society of America)
[32] Stover J C, Schröder S and Germer T A 2012 Upper roughness limitations on the TIS/RMS relationship *Proc. SPIE* **8495** 849503–1–7
[33] Karlsson B and Ribbing C G 1982 Optical constants and spectral selectivity of stainless steel and its oxides *J. Appl. Phys.* **53** 6340–6
[34] Aspnes D E and Studna A A 1983 Dielectric functions and optical parameters of Si, Ge, GaP, GaAs, GaSb, InP, InAs, and InSb from 1.5 to 6.0 eV *Phys. Rev.* B **27** 985–1009
[35] Optosurf Gmbh 2009 Data sheet OS 500-32 Url: www.optosurf.de/images/Datenblaetter/en/Data-Sheet-OS-500.pdf Date accessed: 23 Febrauary 2015
[36] Sensofar-Tech 2009 Sensofar Plu Neox Brochure Url: www.sensofar.com/sensofar/pdf/PLu_neox.pdf Date accesed: 13 Febrauary 2015
[37] Lin T Y, Blunt L and Stout K J 1993 Determination of proper frequency bandwidth for 3D topography measurement using spectral analysis. Part I: isotropic surfaces *Wear* **166** 221–32
[38] Pawlus P 2007 Digitisation of surface topography measurement results *Meas. J. Int. Meas. Confed.* **40** 672–86
[39] Karamehmedović M, Hansen P-E and Wriedt T 2013 An efficient rough-interface scattering model for embedded nano-structures *Thin Solid Films* **541** 51–6
[40] Schröder S, Duparré A, Coriand L, Tünnermann A, Penalver D H and Harvey J E 2011 Modeling of light scattering in different regimes of surface roughness *Opt. Express* **19** 9820–35
[41] Nilsson A M and Jonsson J C 2010 Light-scattering properties of a venetian blind slat used for daylighting applications *Sol. Energy* **84** 2103–11
[42] Breault Research Organization Inc 2012 Scattering in ASAP Url: www.breault.com/sites/default/files/knowledge_base/brotg0922_scatter.pdf Date accessed: 16 Febrauary 2015
[43] Freniere E R, Gregory G G, Chase R C and Corporation L R 2004 Interactive software for optomechanical modeling *Proc. SPIE Optomech. Eng.* **3130** 128–33
[44] Asmail C 1991 Bi-directional scattering distribution function (BSDF): a systematized bibliography *J. Res. Natl Inst. Stand. Technol.* **96** 215–23